

## Improved of Stability of PMSG-Wind Generator Using Fact Device



**Shaik Madar Saheb**  
M.Tech Student,  
Department of EEE,  
Vijaya Engineering College,  
Ammapalem(v),konijarla(m),  
Khammam, Telangana State, India.



**Shahima Sherien**  
Assistant Professor,  
Department of EEE,  
Vijaya Engineering College,  
Ammapalem(v),konijarla(m),  
Khammam, Telangana State, India.

### Abstract:

This paper presents the stability-improvement results of four parallel-operated offshore wind turbine generators (WTGs) connected to an onshore power system using a static synchronous compensator (STATCOM). The operating characteristics of each of the four WTGs are simulated by a 5-MW wind permanent-magnet synchronous generator while the onshore power system is simulated by a synchronous generator (SG) fed to an infinite bus through two parallel transmission lines. A damping controller of the proposed STATCOM is designed by using a pole-assignment approach to render adequate damping to the dominant modes of the studied SG. A frequency-domain approach based on a linearized system model using eigenvalue analysis is performed while a time-domain scheme based on a nonlinear system model subject to disturbances is also carried out. It can be concluded from the simulation results that the proposed STATCOM joined with the designed damping controller can effectively improve the stability of the studied SG-based onshore power system under various disturbance conditions.

### Index Terms:

Dynamic stability, permanent-magnet synchronous generator (PMSG), pole-assignment approach, static synchronous compensator, wind turbine generator (WTG).

### I. INTRODUCTION:

RENEWABLE energy is one of the hottest themes in the entire world today due to the fast and huge consumption of fossil fuels. Some academic researchers have devoted to high-capacity offshore wind turbine generators (WTGs) connected to onshore substations through under-sea cables.

Currently, wind doubly-fed induction generators (DFIGs) and wind permanent-magnet synchronous generators (PMSGs) have been widely used in high-capacity offshore wind farms (OWFs). From the historical point of view, a direct-coupled, modular PMSG for variable-speed wind turbines was proposed and multiple single-phase outputs were separately rectified to obtain a smooth dc-link voltage [1]. The dynamic model based on small-signal stability of a wind turbine (WT) using a direct-drive PMSG with its power converters and controllers was proposed in [2]. A new interconnecting method for two or more PMSG-based WTGs used in a wind farm was proposed in [3], and the proposed scheme required only one externally commutated inverter and only one dc link. A small-signal 47th-order analytical model for representing the operating characteristics of a direct-drive PMSG connected to ac grids of widely varying strength and very weak grids was explored in [4]. A variable-speed WT-PMSG connected to the power grid through a fully controlled frequency converter has the reactive-power control ability to offer required reactive power of the fixed-speed WT generators connected in series or parallel to its terminals [5]. The control strategy of a hybrid wind farm containing a large number of induction machine (IM)-based WTGs and very few PMSG-based WTGs to compensate the reactive power requirement of the IM during faults and mitigate power fluctuations during wind gusts was proposed in [6]. An integration of a generator-side three-switch buck-type rectifier and a grid-side Z-source inverter as a bridge between the PMSG and the grid was proposed for a PMSG-based WTG while the experimental validation and simulation studies were carried out to examine the effectiveness of the proposed scheme [7]. A simple coordinated control of dc-link voltage and pitch angle of a PMSG-based WTG to smooth wind power fluctuations was proposed [8].

Regarding the applications of STATCOM to power-system stability improvement, the stability enhancement of power systems using STATCOMs and the damping controller design of STATCOMs were presented in [9]. A variable-blade pitch of a WTG and design of an output feedback linear quadratic controller for a STATCOM to perform mechanical power control and voltage control under different operating conditions were studied in

[10]. Controller design and system modeling for quick load voltage regulation and suppression of voltage flicker using a STATCOM were explored in [11]. A novel D-STATCOM control algorithm for enabling separate control of positive- and negative-sequence currents was proposed in [12]. Dynamic characteristics of a power system with a STATCOM and a static synchronous series compensator

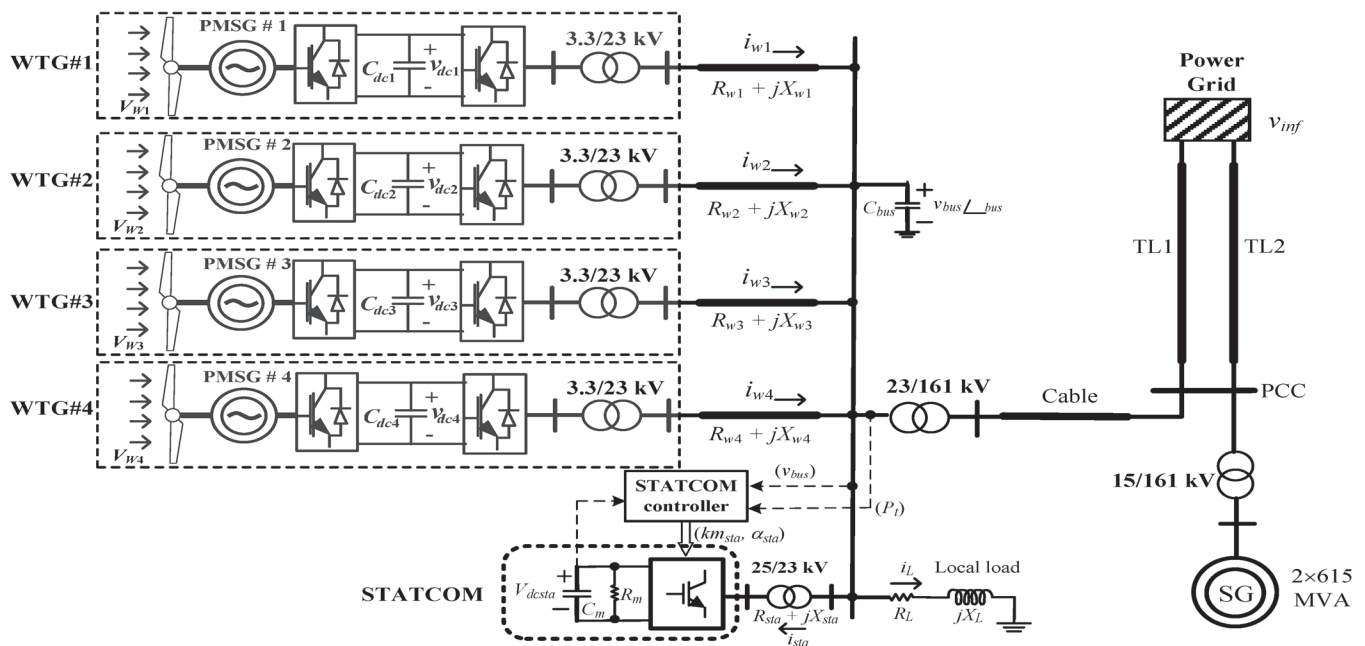


Fig. 1. Configuration of the studied SG-based OMIB system containing four parallel-operated PMSG-based WTGs with STATCOM.

Basically, the grid-side converter of the PMSG-based WTG can be operated as a STATCOM. Many manufacturers also provide this option even for the case when the WTG is not running. But in a real PMSG-based OWE, it has several PMSG-based WTGs operating together, and it is difficult to control reactive power of all WTGs at the same time to supply adequate reactive power to the system. Hence, to guarantee good power quality (PQ) of the system, an additional VAR compensator is required. In this paper, a STATCOM is proposed as a VAR compensator. (SSSC) through digital simulations were compared in [13]. The application of a STATCOM to damp torsional oscillations of a series-capacitor compensated ac system were shown in [14]. The characteristics of using PSS, static VAR compensator (SVC), and STATCOM for damping undesirable interarea oscillations of a power system were compared in [15]. These days, with the fast advance of high-capacity power-electronics technology, large commercial wind turbine generators can be practically employed to contribute high generated power to power systems, where wind PMSGs with full back-to-

back converters have proven to be good choices for high-power WTGs. This paper focuses on modeling the characteristics of four 5-MW PMSG-based WTGs fed to an SG-based power system to examine the effect of large power penetration to the SG. For improving the damping of the SG of the OMIB system, a STATCOM joined with the designed PID controller connected to the common ac bus of the studied system is proposed.

## II. CONFIGURATION OF THE STUDIED SYSTEM:

Fig. 1 shows the configuration of the studied system. The right-hand side of Fig. 1 represents the synchronous generator (SG)-based one-machine infinite-bus (OMIB) system. Two parallel-operated 615-MVA SGs are connected to an infinite bus (or a power grid) through two parallel transmission lines (TL1 and TL2) and a 15/161-kV step-up transformer [16], [17].

Four parallel-operated PMSG-based WTGs and a 5-MVAR STATCOM are connected to the common offshore ac bus that is fed to the point of common coupling (PCC) of the OMIB system through a step-up transformer of 23/161 kV and a cable (undersea and underground cables). Each 5-MW WTG is represented by a PMSG with an ac/dc converter, a dc link, a dc/ac inverter, and a step-up transformer of 3.3/23 kV. While the shaft of the wind PMSG is directly driven by a variable-speed WT, the four PMSG-based WTGs, the STATCOM, and a local load are connected to a common ac bus through connection lines and transformers. The equivalent capacitance is also connected to the common ac bus. The employed mathematical models of the studied system will be described.

## A. Wind Turbine Model and Mass-Spring-Damper Model :

The captured mechanical power (in watts) by a WT can be written by

$$P_m = \frac{1}{2} \rho \cdot A_1 \cdot V_W^3 \cdot C_p(\lambda, \beta) \quad (1)$$

where  $\rho$  is the air density [kg/m<sup>3</sup>],  $A_1$  is the blade swept area [m<sup>2</sup>],  $V_W$  is the wind speed (in meters per second), and  $C_p$  is the dimensionless power coefficient of the WT. The  $C_p$  can be expressed by

$$C_p(\lambda, \beta) = \begin{cases} \frac{16}{15} \left( \frac{\lambda - \beta}{\lambda} - \beta - \beta^3 \right) & \text{if } \lambda \leq \lambda_{cut-in} \\ 0 & \text{otherwise} \end{cases} \quad (2)$$

where

$$\lambda = \frac{R_{tip}}{V_W} \cdot \omega_H \quad (3)$$

$$\beta = \frac{1}{\lambda} \quad (4)$$

where  $\omega_H$  is the blade angular speed (in radians per second),  $R_{tip}$  is the blade radius (in meters),  $\lambda$  is the tip speed ratio,

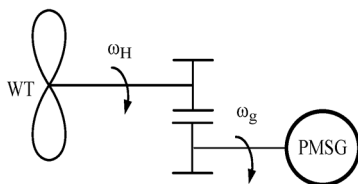


Fig. 2. Two-inertia reduced-order equivalent mass-spring-damper model of each WT coupled to the rotor shaft of a wind PMSG.

$\beta$  is the blade pitch angle (in degrees), and  $\lambda_{cut-in}$  and  $\lambda_{cut-out}$  are the constant coefficients for  $C_p$ . The wind speed  $V_W$  is modeled as the algebraic sum of a base wind speed, a gust wind speed, a ramp wind speed, and a noise wind speed [18] while the expression of  $C_p$  can be referred to [19]. The cut-in, rated, and cut-out wind speeds of the studied WT are 4, 14, and 25 m/s, respectively. When wind speed  $V_W$  is lower than 14 m/s,  $\beta = \beta_{min}$ . When  $V_W > 14$  m/s, the pitch-angle control system activates and  $\beta$  increases accordingly. Each WT is directly coupled to the rotor shaft of a wind PMSG and it can be represented by a two-inertia reduced-order equivalent mass-spring-damper model shown in Fig. 2 [20]–[22].

The per-unit (p.u.) equations of motion for the two-inertia reduced-order WT model are expressed by

$$J_H \frac{d\omega_H}{dt} = T_m - K(\theta_H - \theta_P) - D(\omega_H - \omega_P) \quad (5)$$

$$J_P \frac{d\omega_P}{dt} = K(\theta_H - \theta_P) + D(\omega_H - \omega_P) - T_e \quad (6)$$

$$p \theta_H = \omega_H - \omega_P \quad (7)$$

where  $p$  is the differential operator with respect to time  $t$ ;  $J_H$  and  $J_P$  are the inertias of the hub and the PMSG, respectively;  $\omega_H$  and  $\omega_P$  are the angular speeds of the hub and the PMSG, respectively;  $D$ ,  $K$ , and  $\theta_H - \theta_P$  are the mechanical damping coefficient, spring constant, and rotor-angle difference between the hub and the PMSG, respectively;  $T_m$  and  $T_e$  are the mechanical input torque and the electromagnetic torque of the PMSG, respectively [21].

## B. Permanent-Magnet Generator and Power Converters

The p.u.  $d-q$  axis equivalent circuit model of the studied wind PMSG, where the  $d$ -axis is fixed on the machine rotor and rotates at rotor speed, can be expressed by [16] and [17]

$$u_d = -r_s i_d + \frac{p\psi_d}{\omega_g} + \frac{\omega_g}{\omega_g} \psi_q \quad (8)$$

$$u_q = -r_s i_q + \frac{p\psi_q}{\omega_g} - \frac{\omega_g}{\omega_g} \psi_d \quad (9)$$

where

$$\psi_d = -X_{ls} i_d + X_{lm} i_m - X_{ld} i_f \quad (10)$$

$$\psi_q = -X_{ls} i_q + X_{lm} i_m + X_{mq} i_f - X_{ld} i_f + X_{mq} i_m \quad (11)$$

where  $\psi$  is the per-unit flux linkage,  $u$  is the per-unit stator winding voltage,  $i$  is the per-unit stator winding current,  $X_{ls}$  is the per-unit magnetization reactance,  $X_{lm}$  is the per-unit leakage reactance,  $i_m$  is the

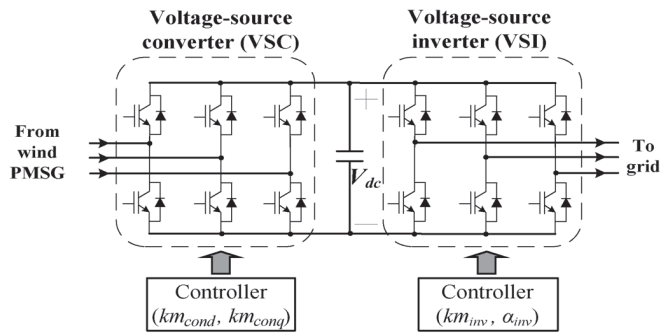


Fig. 3. Model of power converters of the studied wind PMSG.

per-unit rotational speed, and  $\omega_r$  is the per-unit base speed. The power converter of each wind PMSG consists of a voltage- source converter (VSC) and a voltage- source inverter (VSI) as shown in Fig. 3. The VSC or the VSI consists of six insulated-gate bipolar transistors (IGBTs). The common dc link with a large capacitor is connected between the VSC and the VSI. The operation of the VSC and the VSI is properly decoupled by the dc-link capacitor and, hence, the VSC and the VSI have independent controllers.

The input  $d-q$  axis per-unit voltages of the voltage-source converter (VSC) can be expressed by  $v_{d,inv} = V_{dc} m_{d,inv} \cos(\alpha_{inv})$  and  $v_{q,inv} = V_{dc} m_{q,inv} \sin(\alpha_{inv})$ , respectively, where  $V_{dc}$  is the dc-link voltage while  $m_{d,inv}$  and  $m_{q,inv}$  are the  $d$ - and  $q$ -axis modulation indices of the VSC converter, respectively. The output  $d-q$  axis per unit voltages of the VSC inverter of a wind PMSG can be written by  $v_{d,inv} = V_{dc} m_{d,inv} \cos(\alpha_{inv})$  and  $v_{q,inv} = V_{dc} m_{q,inv} \sin(\alpha_{inv})$ , respectively, where  $m_{d,inv}$  and  $m_{q,inv}$  are the modulation index and the phase angle of the VSC inverter, respectively. The fundamental control block diagram of the VSC converter and the VSC inverter of each of the wind PMSGs can be referred to Fig. 4. Fig. 4 shows that  $\omega_r$  is responsible to control the rotor speed of the wind PMSG,  $Q_{ref}$  is used to control the output reactive power of the PMSG,  $v_{dc}$  is employed to control the dc-link voltage, and  $v_s$  is utilized to control the stator-winding voltage of the PMSG [23].

C.STATCOM Model:

The per-unit  $d$ - and  $q$ -axis output voltages of the proposed STATCOM shown in Fig. 1 can be written by, respectively

$$v_d = V_{dc} m_d \cos(\alpha) \quad (12)$$

$$v_q = V_{dc} m_q \sin(\alpha) \quad (13)$$

where  $v_{d,inv}$  and  $v_{q,inv}$  are the per-unit  $d$ - and  $q$ -axis voltages at the output terminals of the STATCOM, respectively;  $m_{d,inv}$  and  $m_{q,inv}$  are the modulation index and phase angle of the STATCOM, respectively;  $\alpha_{inv}$  is the voltage phase angle of the common ac bus, and  $V_{dc}$  is the per-unit dc voltage of the dc capacitor  $C_{dc}$  [24]. The per-unit dc voltage-current equation of the dc capacitor  $C_{dc}$  can be described by

$$C_{dc} \frac{dv_{dc}}{dt} = I_{d,sta} - V_{dc} - R_{dc} i_{d,sta} \quad (14)$$

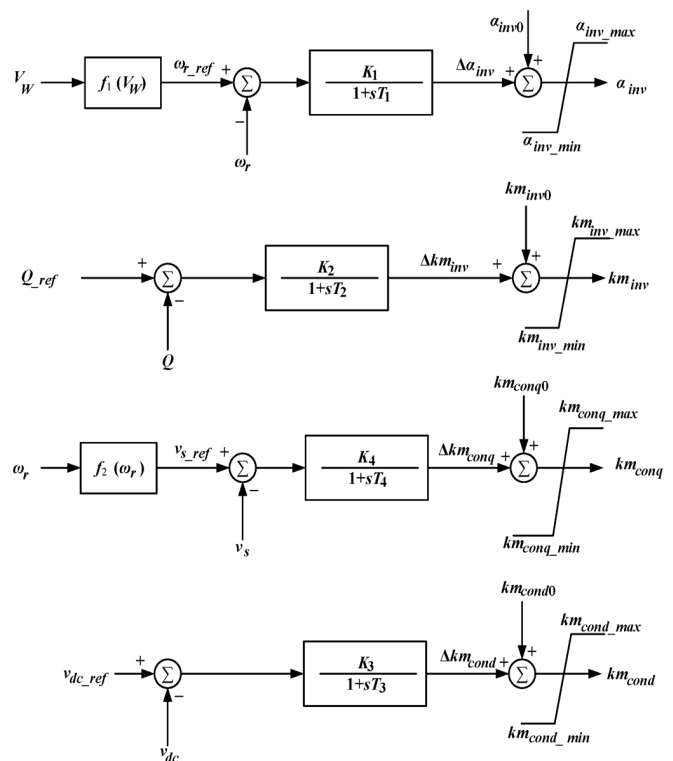


Fig. 4. Control block diagram of the VSC converter and the VSC inverter of each of the wind PMSGs [23].

where

$$I_{d,sta} = i_{q,sta} \cdot km_{sta} \cdot \cos(\theta_{bus} + \alpha_{sta}) + i_{d,sta} \cdot km_{sta} \cdot \sin(\theta_{bus} + \alpha_{sta}) \quad (15)$$

is the per-unit dc current flowing into the positive terminal of  $V_{d,sta}$ ,  $R_m$  is the per-unit equivalent resistance considering the equivalent electrical losses of the STATCOM, and  $i_{q,sta}$  and  $i_{d,sta}$  are the per-unit  $q$ - and  $d$ -axis currents flowing into the terminals of the STATCOM, respectively. The fundamental control block diagram of the employed STATCOM including a proportional-integral-derivative (PID) damping controller is shown in Fig. 5. The per-unit dc voltage  $V_{d,sta}$  is controlled by the phase angle  $\alpha_{sta}$  while the voltage  $v_{sta}$  is varied by changing the modulation index  $km_{sta}$ . Based on the conclusions of [25] and [26],

ulation index  $km_{sta}$ . Based on the conclusions of [25] and [26], the size of the STATCOM in this paper is chosen as  $\pm 5$  MVAR that is equal to 25% of the capacity of the studied OWF. The procedure to calculate parameters of the proposed STATCOM is referred to in [26].

### III. DESIGN OF A PID DAMPING CONTROLLER FOR THE STATCOM USING MODAL CONTROL THEORY:

This section describes the design procedure and design results of the PID damping controller of the proposed STATCOM shown in Fig. 5. The aim of the PID controller for the STATCOM is to achieve stability improvement of the studied SG-based OMIB system with four parallel-operated PMSG-based WTGs. The nonlinear system equations developed in Section II can be linearized around a selected nominal operating point to acquire a set of linearized system equations in matrix form of [27]

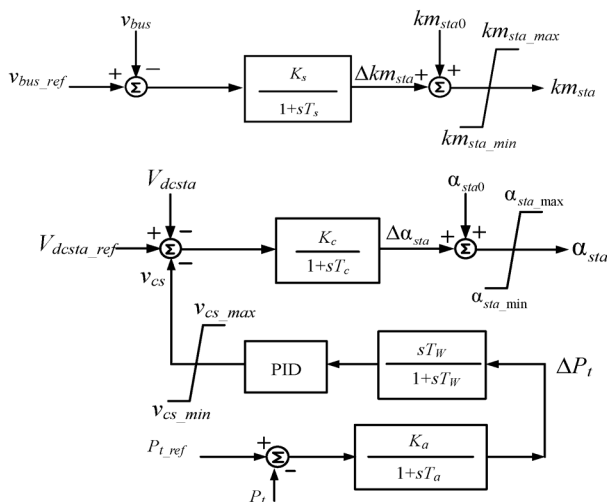


Fig. 5. Control block diagram of the employed STATCOM including the designed PID damping controller [24].

where  $X$  is the state vector,  $Y$  is the output vector,  $U$  is the external or compensated input vector, and  $W$  is the disturbance input vector while  $A$ ,  $B$ ,  $C$ , and  $D$  are all constant matrices of appropriate dimensions. To design the PID STATCOM damping controller shown in Fig. 5,  $W$  in (16) and  $U$  in (17) can be ignored by setting  $D = V = 0$ . The state vector  $X$  in (16) and (17) can be partitioned into four substate vectors as  $X = [X_{WT-PMSG}, X_{OMIB}, X_{LOCAL}, X_{STA}]^T$ , where  $X_{WT-PMSG}$ ,  $X_{OMIB}$ ,  $X_{LOCAL}$ , and  $X_{STA}$  are referred to the system state vectors of the four WT-PMSG sets, the SG-based OMIB system, the local load, and the STATCOM, respectively. Since the wind speed  $V_W$  of the studied WTGs seldom reaches the rated wind speed of 14 m/s,  $V_W$  of 12 m/s is properly selected as the nominal operating point for designing the PID damping controller.

Table I lists the eigenvalues of the studied SG-based OMIB system containing the four PMSG-based WTGs and the STATCOM (but without PID controller) under the selected nominal operating conditions that are:  $P_G = 0.9$  p.u.,  $V_t = 1.0$  p.u.,  $PF = 0.975$  lagging, and  $V_W = 12$  m/s. The eigenvalues ( $) \times n$ , where  $n = 3$  or  $4$ , listed in Table I, represent the repeated eigenvalues of the four WT-PMSG sets since four WT-PMSG sets have identical parameters. Hence, the eigenvalues  $\Lambda_4, \Lambda_5, \Lambda_8, \Lambda_{14}, \Lambda_{17}$ , and  $\Lambda_{25} - \Lambda_{29}$  listed in Table I are related to the modes of the four WT-PMSG sets. The mode  $\Lambda_{12}$  is the eigenvalue that is closest to the imaginary axis in all system eigenvalues but it is nearly fixed on the complex plane and its frequency is around 60 Hz. The eigenvalues  $\Lambda_{20}$  and  $\Lambda_{24}$  listed in Table I refer to the mechanical mode and the exciter mode of the studied SG, respectively. They are the modes of low-frequency oscillations of the OMIB system, and these oscillations are related to the dominant modes of the studied system. Since

TABLE I: EIGENVALUES (RAD/S) OF THE STUDIED SYSTEM UNDER NOMINAL OPERATING CONDITIONS

	System with STATCOM but without PID controller	System with STATCOM and PID controller
$\Lambda_1$	-100	-100
$\Lambda_2$	$-25.727 \pm j89496$	$-25.727 \pm j89496$
$\Lambda_3$	$-32.393 \pm j88736$	$-32.393 \pm j88736$
$\Lambda_4$	$(-4.504 \pm j6.9726 \times 10^5) \times 4$	$(-4.504 \pm j6.9726 \times 10^5) \times 4$
$\Lambda_5$	$(-4.7032 \pm j5.9666 \times 10^5) \times 4$	$(-4.7032 \pm j5.9666 \times 10^5) \times 4$
$\Lambda_6$	$-233.69 \pm j13938$	$-233.69 \pm j13938$
$\Lambda_7$	$-235.81 \pm j10672$	$-235.81 \pm j10672$
$\Lambda_8$	$(-233.75 \pm j8923.1) \times 3$	$(-233.75 \pm j8923.1) \times 3$
$\Lambda_9$	$-36.267 \pm j2047.8$	$-36.766 \pm j2047.8$
$\Lambda_{10}$	$-24.492 \pm j746.93$	$-20.703 \pm j747.32$
$\Lambda_{11}$	$-652.29, -629.07$	$-652.29, -628.88$
$\Lambda_{12}$	$-0.072063 \pm j376.99$	$-0.071912 \pm j376.99$
$\Lambda_{13}$	$-227.25, -131.31$	$-230.62, -133.62$
$\Lambda_{14}$	$(-471.33) \times 3$	$(-471.33) \times 3$
$\Lambda_{15}$	$-12.686 \pm j76.874$	$-12.687 \pm j76.876$
$\Lambda_{16}$	$-92.814 \pm j24.814$	$-95.532 \pm j36.825$
$\Lambda_{17}$	$(-12.52 \pm j76.862) \times 3$	$(-12.52 \pm j76.862) \times 3$
$\Lambda_{18}$	$-99.557, -34.936$	$-101.76, -34.938$
$\Lambda_{19}$	$-1.8089 \pm j11.216$	$-1.7995 \pm j10.87$
$\Lambda_{20}$	$-0.62329 \pm j10.247$	<b><math>-1.5 \pm j10^*</math></b>
$\Lambda_{21}$	$-8.9828 \pm j10.767$	$-8.9863 \pm j10.771$
$\Lambda_{22}$	$-15.803, -0.65861$	$-14.746, -0.64091$
$\Lambda_{23}$	$-100.66 \pm j0.16538$	$-100.63, -99.544$
$\Lambda_{24}$	$-0.59538 \pm j1.5984$	<b><math>-0.65 \pm j1.6^*</math></b>
$\Lambda_{25}$	$(-100.61) \times 3$	$(-100.61) \times 3$
$\Lambda_{26}$	$(-103.53 \pm j17.853) \times 3$	$(-103.53 \pm j17.853) \times 3$
$\Lambda_{27}$	$(-99.528) \times 3$	$(-99.528) \times 3$
$\Lambda_{28}$	$(-2.3609 \pm j22.862) \times 3$	$(-2.3609 \pm j22.862) \times 3$
$\Lambda_{29}$	$(-0.68174) \times 3$	$(-0.68174) \times 3$
$\Lambda_{30}$	$-6.9848$	$-0.8276 \pm j2.2942$

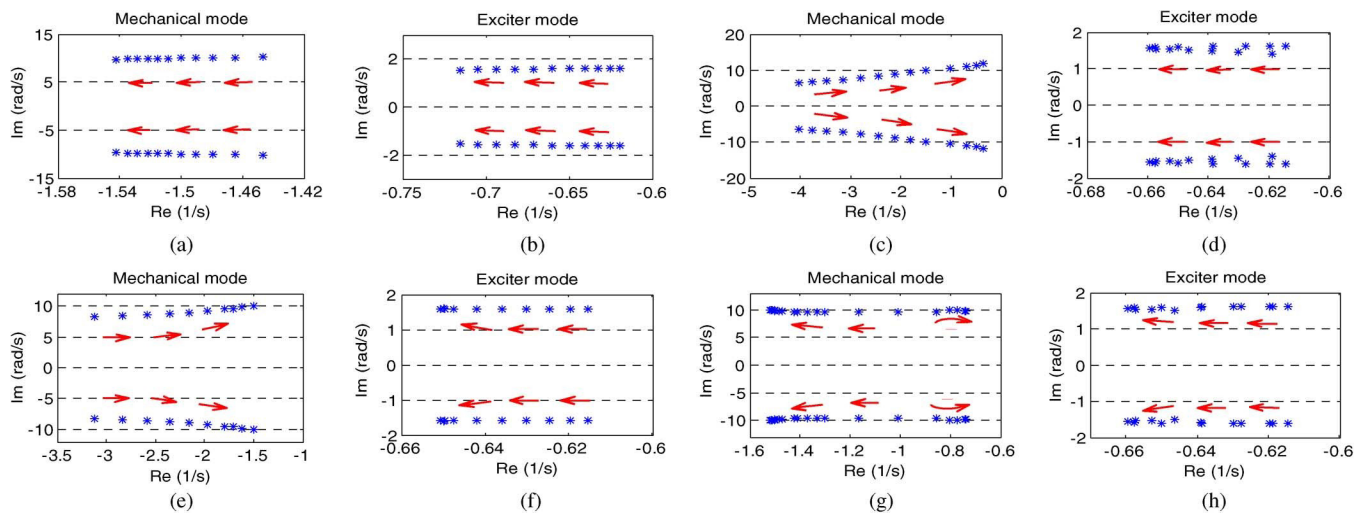
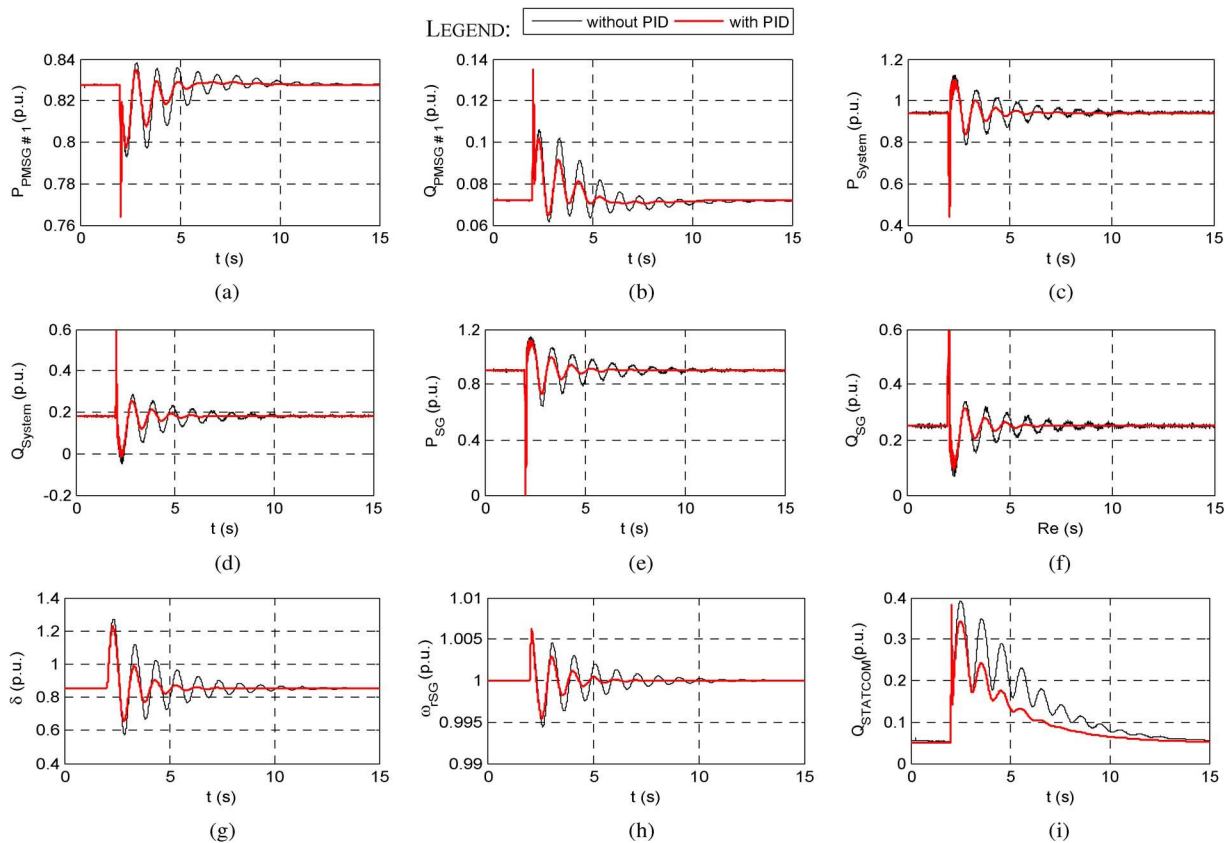


Fig. 6. Steady-state root-loci results of the studied system versus various values of system operating conditions. (a) Mechanical mode versus  $P_G$ . (b) Exciter mode versus  $P_G$ . (c) Mechanical mode versus  $V_t$ . (d) Exciter mode versus  $V_t$ . (e) Mechanical mode versus  $PF$ . (f) Exciter mode versus  $PF$ . (g) Mechanical mode versus  $V_W$ . (h) Exciter mode versus  $V_W$ .

their positions are close to the imaginary axis but not fixed on the complex plane, their damping needs to be improved by using the designed damping controllers. The selection of the two modes is according to the experiences accumulated by the authors for several years [24], [27].

The control block diagram of the phase angle  $\alpha_{sta}$  of the STATCOM including the PID damping controller was shown in Fig. 5. It is seen that the proposed PID damping controller senses the active-power deviation of the transmission line ( $\Delta P_t$ ) to generate a damping signal  $v_{cs}$  in order that the damping char-



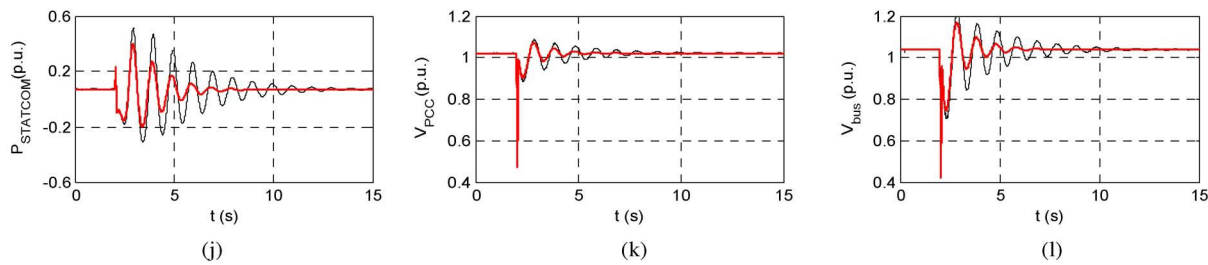


Fig. 7. Transient responses of the studied system with and without the designed PID STATCOM damping controller subject to a three-phase short-circuit fault. (a)  $P_1$ . (b)  $Q_1$ . (c)  $P_{system}$ . (d)  $Q_{system}$ . (e)  $P_{SG}$ . (f)  $Q_{SG}$ . (g)  $\delta$ . (h)  $\omega_{rSG}$ . (i)  $Q_{sta}$ . (j)  $P_{sta}$ . (k)  $V_{PCC}$ . (l)  $v_{bus}$ .

acteristics of the poorly damped mechanical mode  $\Lambda_{20}$  and exciter mode  $\Lambda_{24}$  of the SG listed in Table I can be effectively enhanced. Hence, the output signal in (17) is  $Y = \Delta P_t$  and the input signal in (16) and (17) is  $U = v_{cs}$ . The transfer function  $H(s)$  of the proposed PID STATCOM damping controller in  $s$  domain is given by

$$H(s) = \frac{U(s)}{Y(s)} = \frac{v_{cs}(s)}{\Delta P_t(s)} = \frac{sT_W}{1 + sT_W} \left( K_P + \frac{K_I}{s} + sK_D \right) \quad (18)$$

where  $T_W$  is the time constant of the wash-out term while  $K_P$ ,  $K_I$ , and  $K_D$  are the proportional gain, integral gain, and derivative gain of the damping controller, respectively. Taking the Laplace transformation of (16)–(17), an algebraic equation of the closed-loop system containing the PID STATCOM damping controller can be acquired. The input signal in the  $s$  domain can be expressed by

$$U(s) = H(s)\Delta P_t(s) = H(s)Y(s) = H(s)CX(s). \quad (19)$$

Combining (18) and (19), it yields

$$sX(s) = \{A + B[H(s)C]\} X(s). \quad (20)$$

The characteristic equation of the closed-loop system, including the PID damping controller, is given by

$$\det \{sI - [A + BH(s)C]\} = 0. \quad (21)$$

When two pairs of the prespecified mechanical mode and exciter mode ( $\Lambda_{20}$  and  $\Lambda_{24}$ ) are substituted into (21), the four parameters of the PID controller can be solved. The design results of the PID STATCOM damping controller are given as follows.

*Prespecified eigenvalues*

$$\Lambda_{20} = -1.5 \pm j10.0 \text{ (Mechanical mode of SG)}$$

$$\Lambda_{24} = -0.65 \pm j1.6 \text{ (Exciter mode of SG)}$$

*Parameters of the designed PID damping controller*

$$K_P = -1.17, K_I = -62.2, K_D = -0.51, T_W = 1.16 \text{ s.}$$

The system eigenvalues of the studied SG-based OMIB system containing the four WT-PMSG sets, the proposed STATCOM, and the designed PID damping controller are listed in the third column of Table I. It can be clearly observed that  $\Lambda_{20}$  and  $\Lambda_{24}$  have been exactly located on the desired locations on the complex plane. Some major constraints for selecting the assigned eigenvalues can be referred to in [24]. From the

eigenvalue results listed in the third column of Table I and the four parameters of the designed PID damping controller, it can be concluded that the design results are appropriate to the studied system. Steady-state analysis of the mechanical mode and exciter mode under different operating conditions using root-loci scheme will be performed in the next section.

The design procedure for the PID damping controller is easily understandable, systematic, and useful. One of the main advantages of this design approach is that the proposed PID damping controller can be easily designed by exactly assigning the dominant modes of the studied system to the desire locations of the complex plane. In fact, PID controllers have been practically applied to industry process control and various systems or devices. The main drawback of this method in a real system comes from the fact that the parameters of the controller must be carefully tuned since uncertainty could exist in the studied systems. To perform this task, advanced knowledge for setting up such PID controllers is required to avoid errors, or an autotuning method has to be employed. It is common that commercial PID controllers offer autotuning functions. The operators can start the autotuning functions via some buttons and/or menu choices on the PID controllers. The controllers then automatically execute preplanned experiments on the uncontrolled processes or the control systems depending on the autotuning method implemented. Although other robust control techniques can be more effective than PID controllers, PID controllers still can be practically employed in various control systems with acceptable accuracy. Moreover, a robust controller requires much time to design since system uncertainties have to be included in the design process while robust controllers are not widely applied to practical systems.

#### IV. ROOT-LOCI ANALYSIS

This section presents the root-loci analyzed results of both mechanical mode and exciter mode of the SG when the operating conditions are widely varied. The simulated wind speed  $V_W$  of the four PMSG-based WTGs increases from 4 (cut-in wind speed of WT) to 24 m/s (cut-out wind speed of WT) with a step-wise change of 1 m/s. The output active power of the SG ( $P_G$ ) is increased from 0.5 to 1.5 pu, the terminal voltage of the SG ( $V_t$ ) is increased from 0.8 to 1.2 pu, and the output power factor of the SG ( $PF$ ) is increased from 0.6 to 0.975 lagging. Fig. 6 plots the root-loci results of the mechanical mode and the exciter mode of the SG under the selected operating conditions. Each start symbol (\*) in Fig. 6 presents one wind-speed condition. The root-loci results shown in Fig. 6 are analyzed as

- a) Fig. 6(a) and (b) shows the root-loci results of the mechanical mode and the exciter mode under different values of  $P_G$ , respectively. It is found that mechanical mode and exciter mode always move away from the imaginary axis, and they can be maintained stable by the control scheme when  $P_G$  increases. When  $P_G$  increases, the imaginary parts of mechanical mode and exciter mode are nearly fixed.
- b) Fig. 6(c) and (d) illustrates the root-loci characteristics of the mechanical mode and the exciter mode under different values of  $V_t$ , respectively. It is seen that mechanical mode moves toward the imaginary axis while the exciter mode moves away from the imaginary axis when  $V_t$  increases. Both modes can be stably operated by the control scheme when  $V_t$  changes. When  $V_t$  increases, the imaginary part of the mechanical mode is slightly increased, but the imaginary part of the exciter mode is nearly fixed.
- c) Fig. 6(e) and (f) plots the root-loci outcomes of the mechanical mode and the exciter mode under different values of  $PF$ , respectively. It is observed that, again, the mechanical mode moves toward the imaginary axis while the exciter mode moves away from the imaginary axis when  $PF$  increases. Both modes can be kept stable operation by the control scheme when  $PF$  changes. Again, when  $PF$  increases, the imaginary part of the mechanical mode is slightly increased, but the imaginary part of the exciter mode is nearly fixed.
- d) Fig. 6(g) and (h) draws the root-loci results of the mechanical mode and the exciter mode under different values of  $V_W$ , respectively. It is discovered that the mechanical mode moves away from the imaginary axis when  $V_W$  is increased from the cut-in wind speed to the rated wind speed. However, the mechanical mode moves toward the imaginary axis when  $V_W$  is increased from the rated wind speed to the cut-out wind speed. The exciter mode always moves away from the imaginary axis when  $V_W$  increases. When  $V_W$  increases, both modes can be maintained stable by the control scheme.

## V. TIME-DOMAIN SIMULATIONS:

This section utilizes the nonlinear system model developed in Section II to compare the damping characteristics contributed by the proposed STATCOM joined with the designed PID damping controller. To examine the effectiveness of the proposed damping control scheme, this paper uses a three-phase short-circuit fault suddenly applied to the power grid at 2 s, and the fault is cleared at 2.1 s. Although this type of fault seldom occurs in practical power systems, it is the most critical and the most severe fault to test stability of power systems. Most transient stability studies or evaluations employ such three-phase short-circuit faults applied to the studied systems to check whether the studied systems can withstand such severe system impacts.

Besides, a three-phase short-circuit fault imposes the most severe duty on power circuit breakers while this type of fault is also used to determine the circuit-breaker ratings. Hence, it is worth using a three-phase short-circuit fault for testing the transient responses of the studied systems. If the studied systems are stable when this severe fault is suddenly applied and is cleared by some protective relays, it means that the studied systems have the ability to remain in stable operation when the systems are subject to other faults, such as single line-to-ground fault, line-to-line fault, etc. It is assumed that the studied system operates under the operating conditions used in Table I. Fig. 7 plots the comparative transient responses of the studied system with and without the designed PID damping controller. Since four parallel-operated PMSG-based WTGs have identical parameters and operating conditions, only the active power and the reactive power of WTG#1 are shown in Fig. 7. It is clearly observed from the comparative transient simulation results shown in Fig. 7 that all transient responses of the studied system with the proposed STATCOM joined with the designed PID damping controller can be recovered to the prefault steady-state operating conditions around 6.75 s. When the fault occurs, large amplitudes on all quantities shown in Fig. 7 can be clearly found. It also shows that the proposed STATCOM joined with the designed PID damping controller can supply proper reactive power to the system and offer better damping characteristics to the modes of the SG to quickly damp out the inherent oscillations of the SG. It shows that better damping characteristics can be effectively contributed by the designed PID damping controller of the STATCOM to suppress oscillations of the SG. A voltage profile of the studied system can also be improved by the proposed STATCOM with the designed PID damping controller.

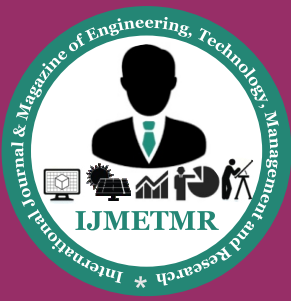
## VI. CONCLUSION:

This paper has presented the stability improvement of four parallel-operated PMSG-based WTGs connected to an SG-based OMIB system. The STATCOM is proposed and is connected to the common ac bus of the four WTGs to supply adequate reactive power and offer proper damping. A PID damping controller has been designed for the STATCOM using modal control theory to assign the mechanical mode and the exciter mode of the studied SG on the desired locations on the complex plane.

Root-loci plots under various operating conditions and time-domain transient simulations of the studied system subject to a three-phase short-circuit fault at the power grid have been systematically performed to demonstrate the effectiveness of the proposed STATCOM joined with the designed PID damping controller on suppressing inherent SG oscillations and improving system stability under different operating conditions. It can be concluded from the simulation results that the proposed STATCOM joined with the designed PID damping controller has the ability to improve the performance of the studied multiple PMSG-based WTGs connected to an SG-based power system under different operating conditions.

## REFERENCES:

- [1] Z. Chen and E. Spooner, "A modular, permanent-magnet generator for variable speed wind turbines," in Proc. 7th Int. Conf. Elect. Mach. Drives, Durham, U.K., Sep. 11–13, 1995, pp. 453–457.
- [2] F. Wu, X.-P. Zhang, and P. Ju, "Small signal stability analysis and control of the wind turbine with the direct-drive permanent magnet generator integrated to the grid," *Elect. Power Syst. Res.*, vol. 79, pp.1661–1667, 2009.
- [3] S. Nishikata and F. Tatsuta, "A new interconnecting method for wind turbine/generators in a wind farm and basic performances of the integrated system," *IEEE Trans. Ind. Electron.*, vol. 57, no. 2, pp. 468–475, Feb. 2010.
- [4] N. P. W. Strachan and D. Jovcic, "Stability of a variable-speed permanent magnet wind generator with weak AC grids," *IEEE Trans. Power Del.*, vol. 25, no. 4, pp. 2779–2788, Oct. 2010.
- [5] S. M. Mueen, R. Takahashi, T. Murata, and J. Tamura, "A variable speed wind turbine control strategy to meet wind farm grid code requirements," *IEEE Trans. Power Syst.*, vol. 25, no. 1, pp. 331–340, Jan. 2010.
- [6] A. E. Leon, J. M. Mauricio, A. Gomez-Exposito, and J. A. Solsona, "An improved control strategy for hybrid wind farms," *IEEE Trans. Sustain. Energy*, vol. 1, no. 3, pp. 131–141, Oct. 2010.
- [7] S. Zhang, K.-J. Tseng, D. M. Vilathgamuwa, T. D. Nguyen, and X.-Y. Wang, "Design of a robust grid interface system for PMSG-based wind turbine generators," *IEEE Trans. Ind. Electron.*, vol. 58, no. 1, pp.316–328, Jan. 2011.
- [8] A. Uehara, A. Pratap, T. Goya, T. Senjyu, A. Yona, N. Urasaki, and T. Funabashi, "A coordinated control method to smooth wind power fluctuations of a PMSG-based WECS," *IEEE Trans. Energy Convers.*, vol. 26, no. 2, pp. 550–558, Jun. 2011.
- [9] H. Chong, A. Q. Huang, M. E. Baran, S. Bhattacharya, W. Litzenberger, L. Anderson, A. L. Johnson, and A. A. Edris, "STATCOM impact study on the integration of a large wind farm into a weak loop power system," *IEEE Trans. Energy Convers.*, vol. 23, no. 1, pp.226–233, Mar. 2008.
- [10] H. Gaztanaga, I. Etxeberria-Otadui, D. Ocnasu, and S. Bacha, "Real-time analysis of the transient response improvement of fixed-speed wind farms by using a reduced-scale STATCOM prototype," *IEEE Trans. Power Syst.*, vol. 22, no. 2, pp. 658–666, May 2007.
- [11] A. Jain, K. Joshi, A. Behal, and N. Mohan, "Voltage regulation with STATCOMs: Modeling, control and results," *IEEE Trans. Power Del.*, vol. 21, no. 2, pp. 726–735, May 2006.
- [12] B. Blažič and I. Papič, "Improved D-STATCOM control for operation with unbalanced currents and voltages," *IEEE Trans. Power Del.*, vol.21, no. 1, pp. 225–233, Jan. 2006.
- [13] A. H. Norouzi and A. M. Sharaf, "Two control schemes to enhance the dynamic performance of the STATCOM and SSSC," *IEEE Trans. Power Del.*, vol. 20, no. 1, pp. 435–442, Jan. 2005.
- [14] K. V. Patil, J. Senthil, J. Jiang, and R. M. Mathur, "Application of STATCOM for damping torsional oscillations in series compensated AC system," *IEEE Trans. Energy Convers.*, vol. 13, no. 3, pp. 237–243, Sep. 1998.
- [15] N. Mithulananthan, C. A. Canizares, J. Reeve, and G. J. Rogers, "Comparison of PSS, SVC, and STATCOM controllers for damping power system oscillations," *IEEE Trans. Power Syst.*, vol. 18, no. 2, pp. 786–792, May 2003.



[16] N. Hatziargyriou, "Modeling new forms of generation and storage," CIGRE Tech. Brochure, TF 38.01.10, Nov. 2000.

[17] P. C. Krause, *Analysis of Electric Machinery*. New York: McGraw- Hill, 1987.

[18] P. M. Anderson and A. Bose, "Stability simulation of wind turbine system," IEEE Trans. Power App. Syst., vol. PAS-102, no. 12, pp.3791–3795, Dec. 1983.

[19] J. G. Sloopweg, H. Polinder, and W. L. Kling, "Representing wind turbine electrical generating systems in fundamental frequency simulations," IEEE Trans. Energy Convers., vol. 18, no. 4, pp. 516–524, Dec.2003.

[20] D. J. Trudnowski, A. Gentile, J. M. Khan, and E. M. Petritz, "Fixed-speed wind-generator and wind-park modeling for transient stability studies," IEEE Trans. Power Syst., vol. 19, no. 4, pp. 1911–1917, Oct.2004.

[21] S. M. Muyeen, M. H. Ali, R. Takahashi, T. Murata, J. Tamura, Y. Tomaki, A. Sakahara, and E. Sasano, "Transient stability analysis of wind generator system with the consideration of multi-mass shaft model," Proc. Int. Conf. Power Electron. Drives Syst., vol. 1, pp.511–516, Jan. 16–18, 2006.

[22] P. Cartwright, L. Holdsworth, J. B. Ekanayake, and N. Jenkins, "Co-ordinated voltage control strategy for a doubly-fed induction generator (DFIG)-based wind farm," Proc. Inst. Elect. Eng., Gen. Transm. Distrib., vol. 151, no. 4, pp. 495–502, 2004.

[23] L. Wang and C.-N. Li, "Dynamic stability analysis of a tidal power generation system connected to an onshore distribution system," IEEE